Journal of Network Intelligence
Taiwan Ubiquitous Information
 ISSN 2414-8105 (Online)
Volume **8**, Number **4**, November **2023**

Maximum Power Development under Varying Solar Radiation Based on Hysteresis-loop Comparison of Selected Duty-cycle Perturbation Algorithms on a Mobility Scooter

Yi-Jui Chiu*

School of Mechanical and Automotive Engineering
Xiamen University of Technology
Xiamen, China
State key laboratory for strength and vibration of mechanical structures
Xi-an, Shaanxi, China
chiuyijui@xmut.edu.cn

Wen-Zhi Wang

School of Mechanical and Automotive Engineering
Xiamen University of Technology
Xiamen, China
2021011034@stu.xmut.edu.cn

Yuh-Chung Hu

Department of Mechanical and Electro-Mechanical Engineer
National Ilan University
I-lan Taiwan
ychu@niu.edu.tw

Shui-Yang Lien

Department of Mechanical and Electro-Mechanical Engineer
National Ilan University
I-lan Taiwan
sylien@xmut.edu.cn

Bing-Rong Zhang

School of Mechanical and Automotive Engineering
Xiamen University of Technology
Xiamen, China
2014110801@xmut.edu.cn

*Corresponding author: Yi-Jui Chiu

Received March 10, 2023, revised May 7, 2023, accepted July 3, 2023.

Abstract. *By analyzing the equivalent circuit model of the photovoltaic cell, a simulation model of the photovoltaic cell was established. To analyze the effects of irradiance and temperature on the output characteristics of the photovoltaic cell, corresponding physical experiments were established in this study to experimentally compare the output characteristics. Meanwhile, in response to the difficulty of achieving relative uniformity in tracking speed and amplitude with the conventional maximum power point tracking algorithm, a hysteresis loop-based algorithm was proposed in this study to select the duty-cycle perturbation. Finally, by comparing it with the conventional algorithm, the following results were obtained: a transient tracking speed of 47 ms, a steady-state oscillation of 0.23 W, and a relative error of 0.12% . These demonstrate the superiority of the algorithm.*
Keywords: Anthropometry of the elderly, Data completion, Thin-plate spline interpolation, Linear interpolation.

1. **Introduction.** Photovoltaic (PV) generation has won worldwide recognition for its reliability, silence, and minimal maintenance requirements. However, the non-linear characteristics of PV cells themselves are vulnerable to environmental impacts. Raising the output efficiency of PV arrays is the key goal of most relevant research; therefore, the implementation of maximum power point tracking (MPPT) is particularly important in PV power generation systems.

Zurbriggen et al. [1] proposed a duty-cycle control strategy that could achieve a balance between MPPT iterations without the need for a converter. The results showed that the combination of a large-signal geometric control strategy and the MPPT concept was suitable for the application of rapid irradiance changes in PV cells. Jately et al. [2] addressed the problem that conventional MPPT algorithms might be inadequate to sense changes in the voltage and current at low irradiance. The resolution of the converter was used as a key constraint to control the performance of the MPPT algorithm. The results showed that the algorithm was able to determine the minimum and optimum values based on the variations of the voltage and current caused by perturbations. Chauhan et al. [3] proposed an improved multi-universe optimization-assisted MPPT algorithm to obtain the maximum power under conditions with partial shading. The results showed that the proposed improved algorithm had advantages over other controller designs in terms of power tracking accuracy, tracking speed, and convergence capability. Bai et al.[4] proposed an improved droop control strategy to further maximize the tracking PV efficiency. The results showed that the proposed method not only improved the stability and power quality of the system but also improved the stability of the control strategy for grid-connected PV operation. Li et al. [5] proposed an MPPT algorithm with diverse meteorological parameters, which analyzed the MPP difference in the presence or absence of a DC/DC converter and served as a rational foundation for the proposed power tracking signal. The results showed the viability and effectiveness of this proposed algorithm control strategy and proved the accuracy of the model. Xu et al. [6] proposed an MPPT technique based on the duty-cycle principle, which adjusted the duty cycle of the converter in tiny steps and thus output the MPP. The results showed that the proposed arithmetic system was more efficient, and its tracking speed was 4.6 times faster than that of the conventional incremental conductance (INC) method. Parr et al. [7] proposed an improved chaotic particle swarm optimization (CPSO) algorithm that extracted the MPP of the PV modules from diverse external conditions. The results showed that the implemented improved chaotic mutation algorithm could overcome the problems captured by the normal particle swarm algorithm into the local MPP. In addition, the proposed algorithm achieved significant improvements in the tracking time, number of iterations, and efficiency. Silveira et al. [8] proposed an improved

extreme-value-seeking control method. The results showed that the proposed method better improved the system efficiency, steady-state power oscillations, and tracking accuracy of the GMPP compared with the classical algorithm. A corresponding improved MPPT algorithm of the proposed algorithm was obtained by optimizing some module parameters of the original algorithm. The experimental and simulation results confirmed that the improved algorithm showed better improvement compared to the previous one. Kihal et al. [9] proposed a new voltage-oriented MPPT method that combined a conventional perturbation observation algorithm with adaptive integral-sliding-mode external voltage control. The results showed that the new algorithm had superior dynamical properties under fast changing irradiation compared to the conventional algorithm. Kota et al. [10] proposed a novel MPPT scheme using linear tangential perturbation observations. The results illustrated that it provided better accuracy, faster tracking times, lower oscillations, and improved steady-state and dynamic performances. Mousa et al. [11] proposed a fast and efficient modular sector algorithm for MPPT. The variable step perturbation algorithm was divided into modular sectors, each with a specific step size. The results showed that the improved algorithm was superior to both the conventional perturbation observation algorithm and the variable step perturbation algorithm. Not only did it improve the initial velocity tracking, but it also minimized the steady-state oscillations. The aforesaid algorithm addressed the inefficiency of the PV system in capturing MPP, and by reasonably adjusting the parameter changes and accessory settings in the PV system, it allowed the PV system to reach a new stable state before the MPPT iteration. The resulted shows that the newly algorithm obtains superior dynamic tracking while keeping simple arithmetic.

Rezk et al. [12] proposed a new method of adaptive and fuzzy logic-based maximum power point (MPP) matching tracking to control PV systems. The experimental results showed that the newly proposed MPPT algorithm was simple, accurate, and could converge to the optimal operating point much faster. Naidoo et al. [13] proposed an MPPT algorithm combining an adaptive neuro-fuzzy inference system (ANFIS) and a microscopically trusted ANFIS-based system. The results showed that the proposed algorithm could better maintain the maximum power of PV tracking and minimize the power fluctuations of the interconnections. Jiang et al. [14] proposed a new hybrid MPPT algorithm to track the MPP of the PV system, which could be tracked without direct current (DC) sensors. The results showed that the novel MPPT algorithm provided an energy improvement of 2.72 % over the conventional perturbation algorithm. Liu et al. [15] proposed a new MPPT algorithm that combined a three-point weighing comparison algorithm and an MPPT inspection scheme. The results showed that the efficiency of the system was 80% when the solar photovoltaic module (SPV) module was overloaded (SPV $>$ load) and 99% when the system was not overloaded (SPV $<$ load), and the proposed algorithm outperformed other conventional algorithms. Mohanty et al. [16] proposed a new hybrid MPPT algorithm, which combined gray wolf optimization and perturbation observation techniques. The results showed that the new MPPT could provide excellent tracking performances under any weather conditions compared with those based on the gray wolf optimization and perturbation observation algorithms. González et al. [17] proposed an optimal design based on the polynomial fitting of surfaces to capture the MPP. The results showed that the proposed strategy was not computationally expensive and proved to be more effective than the conventional algorithm under rigorous testing. Chen et al. [18] proposed an Internet of Things based Computer-Integrated Manufacturing algorithm applied to photovoltaic material characterization. This resolution improved the operational procedures to suit the manufacturing generation manufacturing system.The results

showed that the algorithm efficiently tracked the relationships in the semiconductor manufacturing process, and resulted in higher output power of the PV panels. Peng et al.[19] proposed a bidirectional long- and short-term memory (BiLSTM) depth tilt model to predict the operational trends of temperature, irradiance, and other meteorological conditions. The results showed that the maximum power of PV power consumption based on the predicted temperature, irradiance, and other parameters could be effectively predicted to further improve PV efficiency. Liu et al. [20] proposed an MPPT control strategy based on a temporary stop operation strategy of the boost converter and an advanced three-point weight comparison method. The results showed that the algorithm could reduce the switching and conduction losses and provided a 10 % improvement in the overall conversion efficiency compared to the conventional control algorithm. To capture the inefficiency of MPP in PV systems, the optimization algorithms mentioned above were fused by multiple MPPT algorithms to derive a new MPPT algorithm. The performance deficiencies among the algorithms were compensated to optimize their performance parameters with respect to the original individual algorithms. It showed the resulted MPPT algorithm to be fast, accurate, and able to converge to the maximum operating point relatively quickly. Based on the theoretical analysis of the PV cell, the corresponding PV cell model was established in this study. The results of the output characteristics of PV modules under different environments were analyzed, and the corresponding experimental platform was built for relevant verification. Based on the traditional perturbation algorithm, a selective duty-cycle perturbation algorithm based on hysteresis loop comparison was proposed in this study. This method was used to introduce the link of the hysteresis loop comparison as the basis of the duty-cycle direction judgment. Finally, the traditional algorithm and the improved algorithm were analyzed and compared to illustrate the feasibility of the improved algorithm.

2. **Theoretical model.** Based on the work of Li et al. [21], the equivalent circuit of the PV cell is shown in Figure 1. I_D is the current of the diode inside the PV cell, which can be expressed as follows:

$$I_D = I_0[exp\frac{qU_D}{AKT} - 1]. \tag{1}$$

where I_{ph} is the photo-generated current, I_0 is the P-N junction reverse saturation current of the equivalent diode inside the PV cell, q is the electronic charge, $q = 1.6 \times 10^{-19}$ C, U_D is the terminal voltage of the equivalent diode, A is a constant related to the P-N junction inside the PV cell, K is the Boltzmann constant, $K = 1.38 \times 10^{-18}$ erg/K, and T is the absolute ambient temperature.

The mathematical model of the current and voltage characteristics of the equivalent circuit of the PV cell is as follows:

$$I_L = I_{ph} - I_0[exp(\frac{qU_D}{AKT}) - 1] - \frac{U_D}{R_{sh}}. \tag{2}$$

$$U_D = U_{OC} + I_L R_S \tag{3}$$

$$I_{SC} = I_0[exp(\frac{qU_D}{AKT}) - 1] \tag{4}$$

$$U_{OC} = \frac{AKT}{q}\ln(\frac{I_{SC}}{I_0} + 1) \tag{5}$$

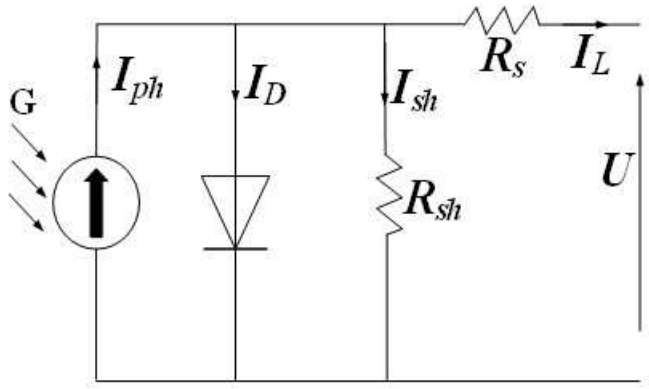

FIGURE 1. Equivalent circuit diagram of photovoltaic (PV) cell [21]

$R_S \to 0$ and $R_{sh} \to \infty$ in the ideal form, and the mathematical model of the simplified equivalent circuit is as follows:

$$I_L = I_{ph} - I_d = I_{ph} - I_0[exp(\frac{qU_D}{AKT}) - 1] \tag{6}$$

The main parameters in the standard environment ($S = 1000$ W/m^2, $T = 25$°C) are the short-circuit current I_{sc}, open-circuit voltage U_{oc}, maximum power voltage U_m, and maximum power current I_m. These four parameters are closely related to the output characteristic curve of the battery, and they can be used to obtain a U-I curve that is similar to the output characteristics. In most engineering models, $I_{ph} = I_{sc}$, $C_1\ I_{SC} = I_0$, and $C_2\ U_{OC} = AKT/q$ are formulated as follows:

$$I_L = I_{SC} - C_1 I_{SC}[exp(\frac{U_L}{C_2 U_{OC}}) - 1] \tag{7}$$

$$C_1 = (1 - \frac{I_m}{I_{SC}})exp(\frac{-U_m}{C_2 U_{OC}}) \tag{8}$$

$$C_2 = (\frac{U_m}{U_{OC}} - 1)[\ln(\frac{1 - I_m}{I_{SC}})]^{-1} \tag{9}$$

El [22] describes that the resistivity of photovoltaic cells drops initially as the temperature rises. After the temperature rises to a certain value, the resistivity stops falling and continues to rise. In addition, with the rise in temperature, the photovoltaic current also rises, which has a negative impact on the conversion efficiency of the cell. López [23] explained that resistivity decreases with increasing irradiance. The efficiency of photovoltaic power generation will increase because of the additional carriers. It is readily apparent that both temperature and irradiance have a critical impact on the efficiency of photovoltaic power generation. The mathematical model in this paper is constructed based on Li′s study. However, for the model to fit the output characteristics of the actual PV cell more closely, the effects brought by irradiance and temperature are considered. Corrections and compensation are made on the basis of the original model, and the corrections for temperature and irradiance are shown below:

$$\Delta T = T - T_{ref} \tag{10}$$

$$\Delta S = \frac{S}{S_{ref}} - 1 \tag{11}$$

It is also necessary to compensate for four parameters (U_m, I_m, U_{oc}, and I_{sc}). T_{ref} and S_{ref} are the temperature and irradiance under standard test conditions, where $T_{ref} = 25°\text{C}$ and $S_{ref} = 1\ \text{kW/m}^2$, respectively, and the corrected I_{sc}, U_{oc}, I_m, and U_m are shown as follows:

$$U_{OC}^* = U_{OC}(1 - b \triangle T)ln(e + \alpha \triangle S) \tag{12}$$

$$U_m^* = U_m(1 - b \triangle T)ln(e + \alpha \triangle S) \tag{13}$$

$$I^* = I_{SC}\frac{S}{S_{ref}}(1 + c\Delta T) \tag{14}$$

$$I_m^* = I_m\frac{S}{S_{ref}}(1 + c\Delta T) \tag{15}$$

In this paper, Equation (10)−(15) are added to Li's mathematical model, which makes the model more realistic, where a is the coefficient of temperature compensation for irradiance, b is the coefficient of temperature compensation for voltage, and c is the coefficient of temperature compensation for current. The values of a, b, and c of the PV cells are often taken as $0.2\ \text{m}^2/\text{W}$, $0.00288\ °\text{C}^{-1}$, and $0.0005°\text{C}^{-1}$ in engineering, and e is the Euler number. Based on the mathematical model established above, a corresponding model was built. The parameters were set as $I_m = 11.28$ A, $I_{sc} = 13$ A, $U_{oc} = 29.5$ V, and U_m= 22.33 V, and they are shown in Figure 2.

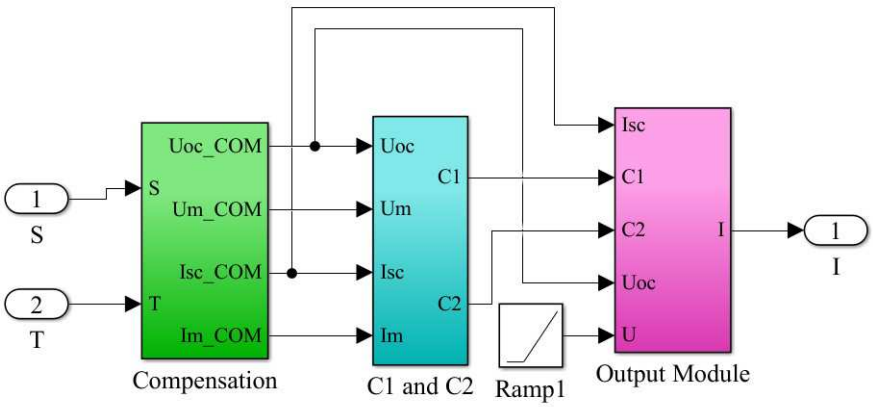

FIGURE 2. PV module model

3. **Output characteristics analysis.** (1) Effect of irradiance on solar panel output

The PV output characteristic curve for the irradiance in the range of 0 to 1200 W/m^2 was obtained at a standard temperature of 25°C, as shown in Figure 3. Figure 3(a) shows the current−voltage contours for different irradiance values. Figure 3(b) shows the voltage−current−irradiance surfaces. Figure 3(c) shows the power−voltage contours for different irradiance values. Figure 3(d) shows the power−voltage−irradiance surfaces. As shown in Figure 3(a) and Figure 3(b), the short−circuit current was smaller with smaller irradiance values, the short-circuit current changed in the range of 0 to 14.7 A, and the volumetric characteristics showed non-linearity overall. When the terminal voltage was 0 to 19.6 V, the short-circuit current maintained a relatively constant value.

When the terminal voltage was 19.6 to 29.5 V, the higher the irradiance was, the faster the current decreased, and a downward slope appeared in the range of 19.6 to

24.1 V. The P_m range in Figure 3(c) and 3(d) was 0 to 312.5 W. Overall, the power output curve showed ramped up first and then underwent a parabolic rapid decline with increasing voltage. When the terminal voltage formed a peak in the 19.6 to 24.1 V interval, the output power and maximum output power increased with the increase in the light irradiance. The terminal voltage of 23.5 V was the MPP. The irradiance had values of 0 to 1200 W/m^2, and the maximum power was 0 to 312.5 W.

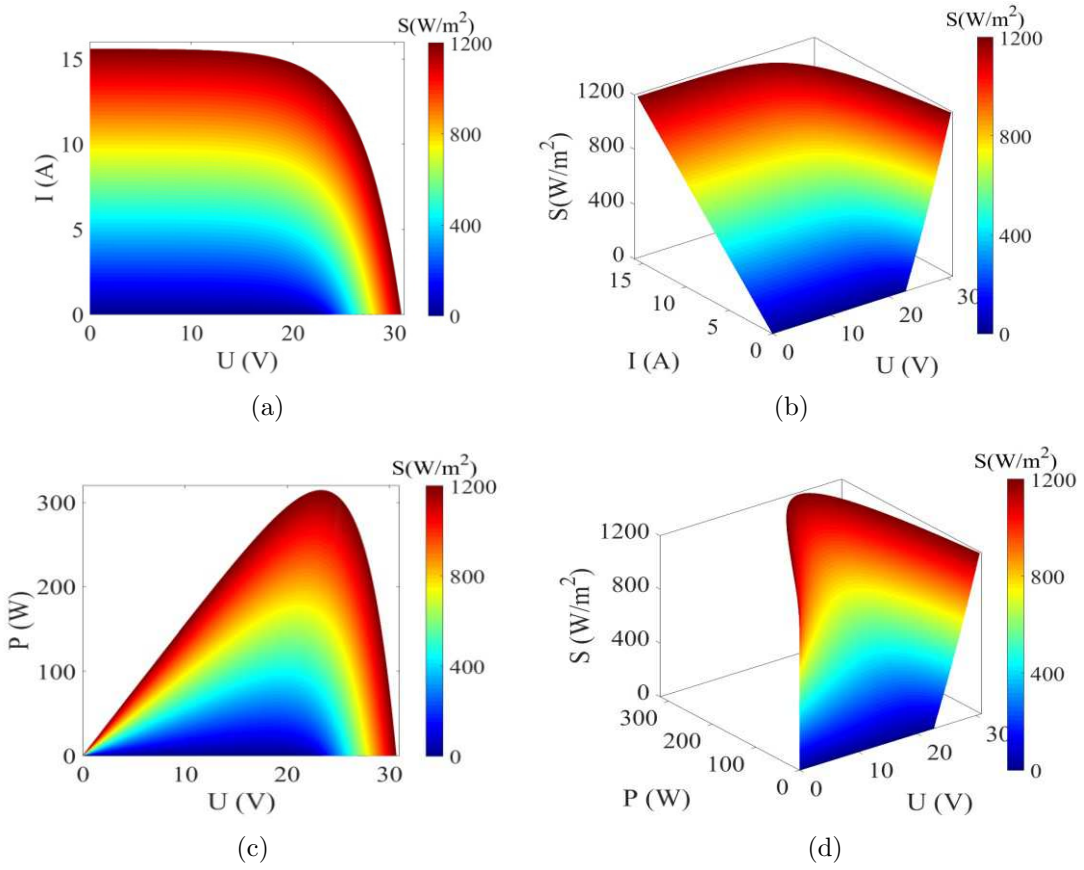

FIGURE 3. PV output characteristics under different irradiance values

(2)Effect of temperature on solar panel output

Under the standard light intensity of 1000 W/m^2, the PV output characteristic curve under the temperature change of 0°C to 100°C was obtained. Figure 4(a) shows the current−voltage contours for different temperatures. Figure 4(b) shows the voltage−current−temperature surfaces. Figure 4(c) shows the power−voltage contours for different temperatures. Figure 4(d) shows the voltage−power−temperature surfaces. As shown in Figure 4(a) and 4(b), the smaller the temperature was, the smaller the short-circuit current and the larger the open circuit voltage became. The variation range of the short-circuit current was 12.1 to 15.5 A and the open circuit voltage was 23.2 to 31.6 V. The overall *I-U* characteristic curve was a "single−knee" curve, and the current output curve showed a parabolic rapid decline after remaining flat. A point of curve inversion appeared in the voltage range of 18.4 to 22.8 V, corresponding to the MPP. The P_m range of Figure 4(c) and 4(d) was 0 to 253.6 W. Overall, with the increase in the voltage, the power output curve increased first and then decreased rapidly in the shape of a parabola. The MPP appeared in the terminal voltage range of 18.4 to 22.8 V. If the temperature was in the range of 0°C to 100°C, the maximum power range was 236.7 to 253.6 W.

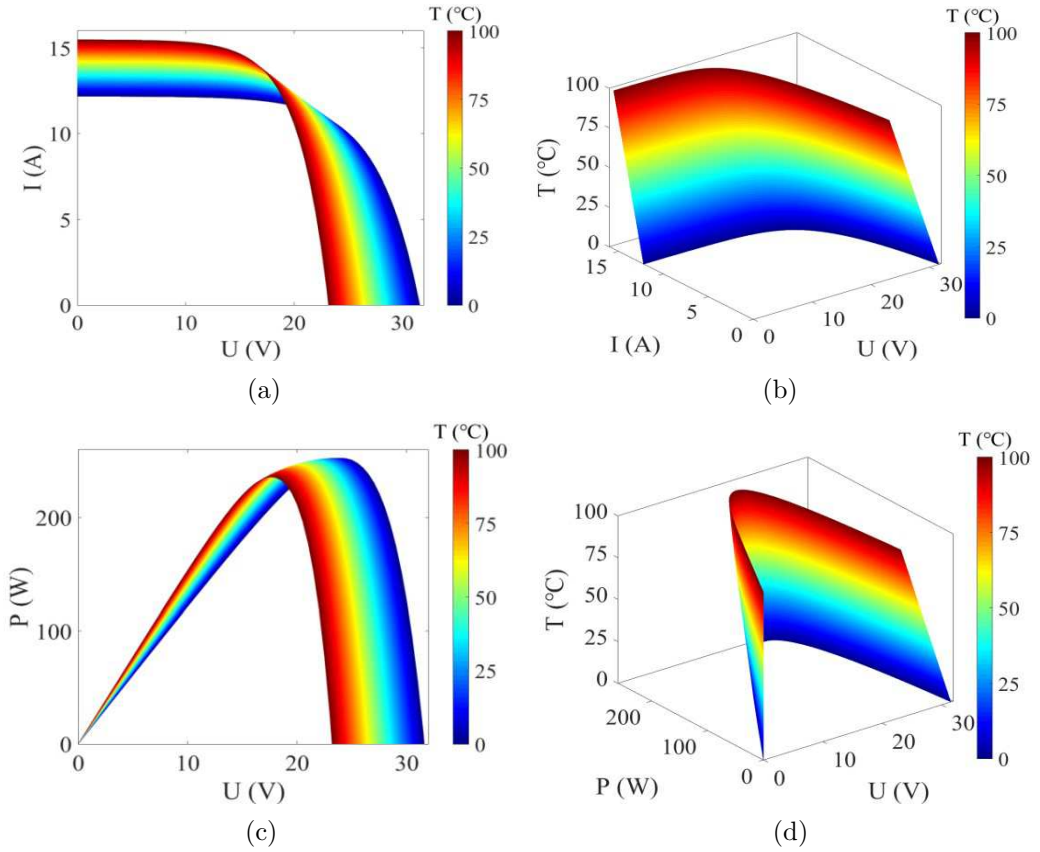

FIGURE 4. PV output characteristics at different temperatures

4. **Experiment.** A photovoltaic power generation system is constructed for the original structure of the mobility scooter in this paper. It is expected that the photovoltaic power generation system installed on the mobility scooter will absorb solar energy, transform solar energy into electrical energy and store it in the battery as an auxiliary energy source, and use solar energy to supply maximum power to the on-board equipment. A physical diagram is shown in Figure 5(a).

The experimental system parameters are shown in Figure 5(b) and Figure 5(c). Experimental equipment comprises the following: (1) photovoltaic module, flexible solar panel model PETC−C252; (2) upper computer, with MATLAB, Simulink, Origin, and other experiment−related software installed; (3) sliding resistor, manual type to adjust the resistance size; (4) multi−meter, to detect the output current and output voltage of the PV module; (5) irradiation meter handheld detection of light intensity, range of 0.1 to 1999.9 W/m^2, accuracy of 0.1 W/m^2; (6) temperature measuring gun infrared handheld, range of −50 to 300°C, accuracy of ±1.5°C; (7) other equipment−wire, screwdriver, electric pen, and other remaining tools. The experimental steps are described as follows: the PV components, sliding rheostat, ammeter, and voltmeter were connected to form a circuit. The resistance of the sliding rheostat was manually adjusted to change the output characteristics of the PV module. A multi−meter was used to detect and sample the output currents and voltages of the PV modules. An irradiance meter was used to measure the irradiance, an infrared thermometer was used to measure the surface temperatures of the modules, and all data points were recorded. The solar cells were placed on horizontal ground, and their irradiance values were measured. When the irradiance tended to a

(a) Solar car physical diagram (b) Outdoor field measuremens

(c) Laboratory bench

FIGURE 5. Experimental system

certain stable natural light condition, the irradiance and temperature of the module surface under different conditions were measured and recorded. Several experiments were conducted to select the best data for analysis, and the data are shown in Table 1.

TABLE 1. Environmental conditions of experiment and simulation

Simulation group	Simulation environment	Experimental group	Experimental environment
Simulation 1	890 W/m^2, 51°C	Experiment 1	890 ± 30 W/m^2, 47−56°C
Simulation 2	630 W/m^2, 47°C	Experiment 2	630 ± 20 W/m^2, 45−51°C
Simulation 3	320 W/m^2, 36°C	Experiment 3	320 ± 20 W/m^2, 35−38°C
Simulation 4	150 W/m^2, 31°C	Experiment 4	150 ± 10 W/m^2, 29−33°C

The experiment and simulation results are compared in Figure 6. The short−circuit currents for the simulated data were I_{sc_Sim1} = 13.1 A, I_{sc_Sim2}= 8.6 A, I_{sc_Sim3} = 4.5 A, and I_{sc_Sim4} = 1.8 A for the four environmental conditions in Figure 6(a).The short-circuit currents of the experimental data were I_{sc_Exp1} = 10.9 A, I_{sc_Exp2} = 7.8 A, I_{sc_Exp3} = 3.5 A, and I_{sc_Exp4} = 1.6 A. The short−circuit currents of the experiments were lower than those of the simulation under the same conditions. The open circuit voltages of the simulation data were U_{oc_Sim1} = 25.1 V, U_{oc_Sim2} = 24.5 V, U_{oc_Sim3} = 23.0 V, and U_{oc_Sim4} = 22.3 V. The open−circuit voltages for the experimental data were U_{oc_Exp1} = 24.9 V, U_{oc_Exp2} = 24.1 V, U_{oc_Exp3} = 23.4 V, and U_{oc_Exp4} = 22.1 V. When the terminal voltage was 0 to 16.6 V, the short-circuit current remained relatively constant. When the terminal charge was 16.6 to 21.3 V, the curve formed a downward slope, and the higher the irradiance was, the faster the current decreasing trend became. Overall, the power

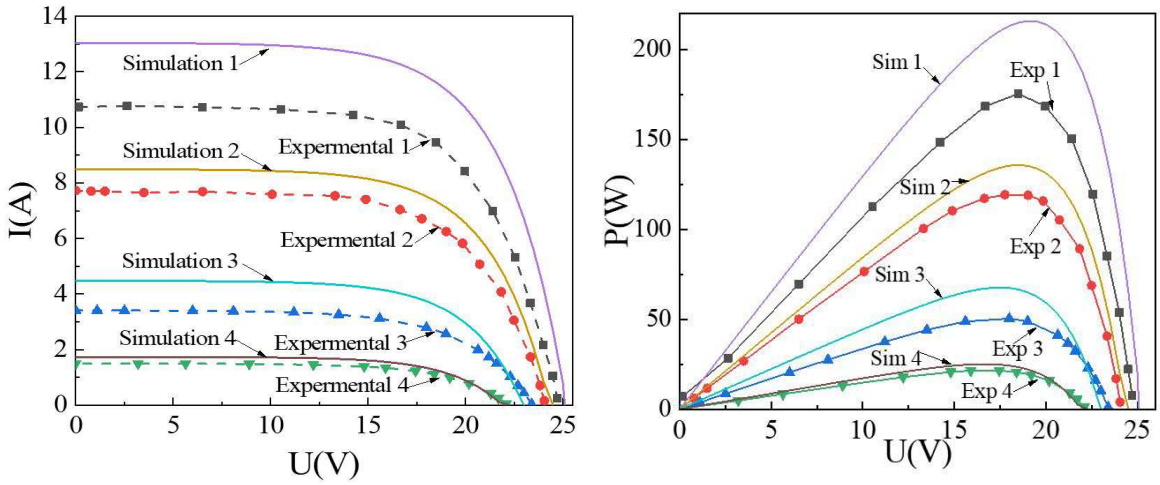

(a) *I-V* comparison chart (b) *P-V* comparison comparison chart

FIGURE 6. Comparison of experimental and simulation data

curve showed the characteristic of maintaining an upward slope and then a parabolic decline, where the highest point was the MPP in Figure 6(b). The maximum points of the simulation curves were $U_{m\_Sim1} = 19.1$ V, $P_{m\_Sim1} = 215.8$ W, $U_{m\_Sim2} = 18.5$ V, $P_{m\_Sim2} = 135.7$ W, $U_{m\_Sim3} = 17.5$ V, $P_{m\_Sim3} = 67.6$ W, $U_{m\_Sim4} = 16.4$ V, and $P_{m\_Sim4} = 25.1$ W. The maximum points of the experimental curves were $U_{m\_Exp1} = 18.5$ V, $P_{m\_Exp1} = 175.3$ W, $U_{m\_Exp2} = 17.7$ V, $P_{m\_Exp2} = 119.2$ W, $U_{m\_Exp3} = 17.9$ V, $P_{m\_Exp3} = 50.3$ W, $U_{m\_Exp4} = 17.1$ V, and $P_{m\_Exp4} = 21.4$ W. There was an error between the simulated and experimental data, which was due to the limitations of the material of the PV cell itself. Furthermore, the experimental conditions of the experiment were not as ideal as the simulated environmental conditions. Many external influencing factors caused differences between the experimental $P-V$ and $I-V$ curves and the output characteristic curves obtained from the simulation. The MPP obtained from the experiment was also smaller than the MPP calculated from the simulation.

5. **Photovoltaic MPPT control system.** Traditional MPPT algorithms include the constant-voltage tracking (CVT) method, the perturb and observe (P&O) method, and the INC method. For the traditional MPPT algorithm, it is difficult to achieve perfect unity of the oscillation amplitude near the operation speed and the MPP. This study explores a novel hysteresis loop comparison−based selective duty-cycle perturbation algorithm to improve the traditional perturbation algorithm.

(1) Duty-cycle perturbation principle

Gupta et al. [24] and Kwan et al. [25] denoted the output terminal voltage as U_0, the load as R_0, the voltage before the boost as V, the duty cycle as D, and the power as P, which was constant before and after the boost. P and U_0 are defined as follows:

$$P = \frac{U_0^2}{R^0} \tag{16}$$

$$U_0 = \frac{1}{1-D}V \tag{17}$$

Equations (16) and (17) can be combined to obtain the following:

$$P = \frac{V^2}{(1-D)^2 R_0} \tag{18}$$

Equations (16)−(18) were applied with irradiance values of 800, 900, and 1000 W/m^2 and an external ambient temperature of 25°C. Figure 7 shows the U-D and P-D curves for these three external conditions. The voltage U decreased as the duty cycle D increased, and the P-D curve showed a single−peaked pattern in all three cases, and the PV system was located at the MPP when the irradiance was 1000 W/m^2 and the duty cycle was $D = 0.76$. When the irradiance was 900 W/m^2, the duty cycle was $D = 0.75$, and the PV system was located at the MPP. When the irradiance was 800 W/m^2, the duty cycle was $D = 0.73$, and the PV system was located at the MPP. If the duty cycle were increased by D, the voltage U and power P would decrease when the PV system was running at the MPP point. If the PV system were operating on the left side of the MPP point, if D increased slightly, the voltage U would tend to decrease, and the power P would approach the MPP. If the PV system were operating on the right side of the MPP, the reverse would be true.

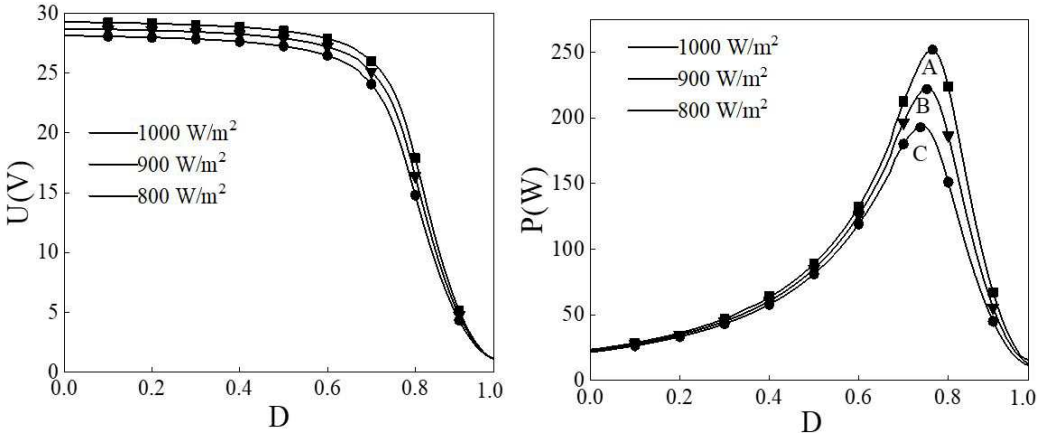

(a) U-D characteristic curves (b) P-D characteristic curves

FIGURE 7. Comparison of experimental and simulation data

(2) Hysteresis comparison

The hysteresis comparison method is based on the principle that the hysteresis loop is composed of two points B and C, which are located at the same distance on both sides of point A, which is the current working point of the PV cell. With point A as the starting point, the perturbation direction provided by the determination of the system could be perturbed to point B and then perturbed in the opposite direction for two steps to reach point C. The power at points A, B, and C are denoted as P_A, P_B, and P_C, respectively. With point A as the center point, if the perturbation direction from point A to point B or from point A to point C is positive, the situation is recorded as "+"; the opposite situation is recorded as "−". The PV power generation system with the addition of the hysteresis loop link will have several possible scenarios, as shown in Figure 8.

$P_{(i-1)}$, $P_{(i)}$, and $P_{(i+1)}$ were calculated using $U_{(i)}$ and $I_{(i)}$. Subsequently, the power values of the three points $i-1$, i, and $i+1$ were compared, and the set accuracy requirement e was used to determine whether the current point reached the MPP that satisfied the accuracy requirement. The following three cases may exist in the tracking process.

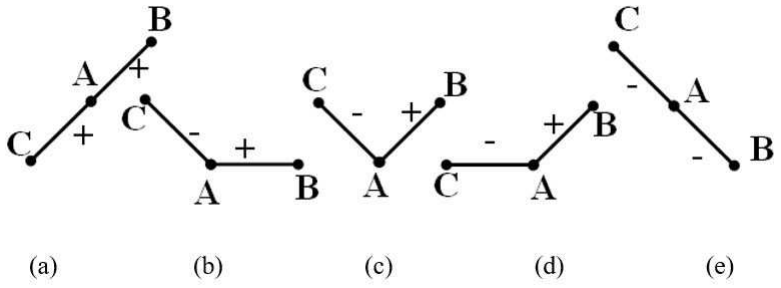

FIGURE 8. Possible scenarios for the hysteresis loop comparison method

1. If $P_{(i-1)} < P_{(i)} \leq P_{(i+1)}$, then $m = 2$, indicating that the power increased with the duty cycle at this time, and a positive (direction of increasing duty cycle) perturbation should be added to obtain the next operating point.

2. If $P_{(i-1)} \geq P_{(i)} > P_{(i+1)}$, then $m = -2$, indicating that the power decreased with the increase in the duty cycle at this time, and the reverse perturbation should be added to obtain the next operating point.

3. In the other cases, $m = 0$, which means that the MPP was between points i-1 and i+1. At this time, $b = Ka$, where K is the adjustment factor for the approximation judgment.

After this tracking was completed, m was cleared, and the process returned to the beginning. The above tracking was repeated until the MPP was tracked to meet the accuracy requirement in Figure 9.

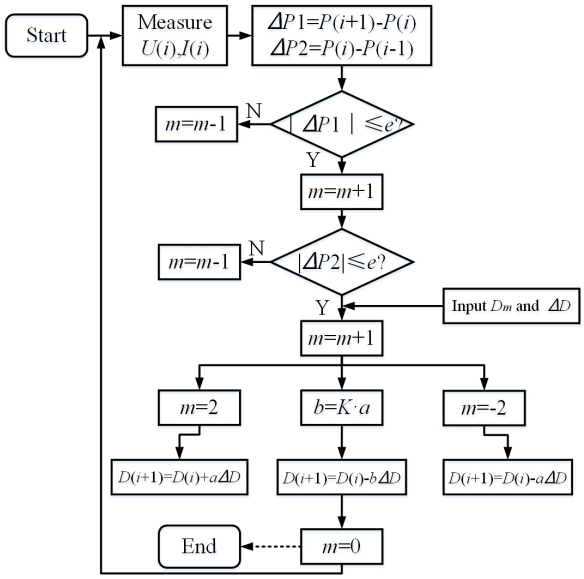

FIGURE 9. Selective duty-cycle perturbation algorithm for hysteresis loop comparison

(3) Simulation analysis

The MPPT simulation model built in the MATLAB/Simulink simulation environment consisted of the following parts: a PV cell module, pulse−width modulation (PWM) signal generator module, DC/DC converter, and MPPT control module, as shown in Figure 10.

The current initial maximum duty cycle was selected to be 0.77. In addition, the simulation time was set to 4 s, and the specific dynamic environment changes and the theoretical output power values are shown in Table 2.

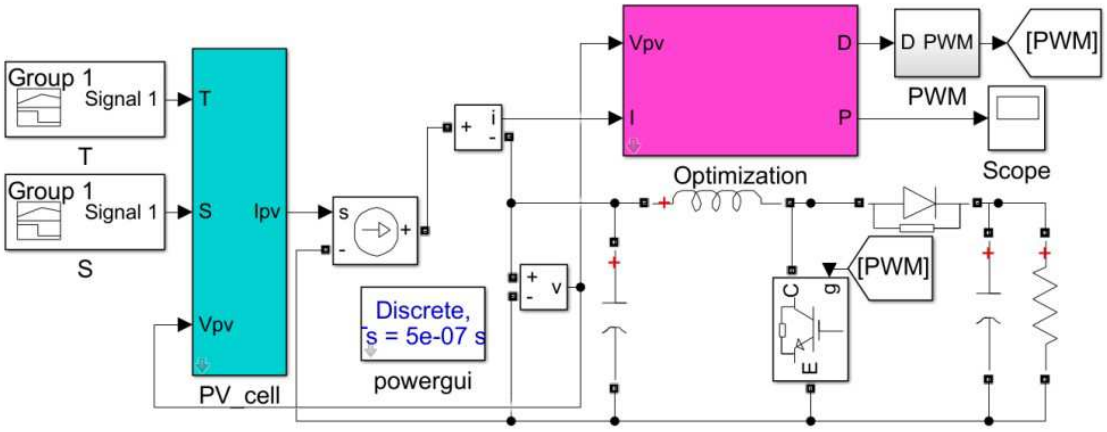

FIGURE 10. Selective duty-cycle perturbation algorithm model for hysteresis loop comparison

TABLE 2. Maximum power output of PV system under dynamic environment

Time (t/s)	0	1	2	3
Temperature (°C)	25	25	25	75
Irradiance (W/m^2)	900	800	1000	1000
Power (W)	221.4	186.6	252.4	233.8

TABLE 3. Performance comparison of the four algorithms

Time (t/s)	Start tracking speed (ms)	Instantaneous tracking speed (ms)
CVT	55	50
P&O	80	72
INC	40	35
Optimization algorithm	55	47
Time (t/s)	Steady-state oscillation (W)	Relative Error (%)
CVT	10.2	5.46
P&O	7.4	3.96
INC	3.3	1.76
Optimization algorithm	0.23	0.12

Figure 11(a) shows the simulation diagram of the CVT method control. In the range of 0 to 3 s, the tracking power and theoretical data fit well, but the oscillation amplitude was large. At 3 s, the temperature rose from 25°C to 75°C. From Table 3 and Figure 11(a), it is obvious that there is an error in work point tracking within 3 to 4 s. The work point in this region should be tracked to approximately 233.8 W, but it is tracked near 105 W. Figure 11(b) shows the output power simulation of the P&O method control. The initial tracking time of this algorithm was slightly long when the irradiance was 900 W/m^2, with fluctuations in the range of 222.3 to 217.2 W and a variation range of about 5.1 W at 0 to 1 s. When the irradiance was 800 W/m^2, the fluctuations were in the range of 185.7 to 181.3 W, with a variation range of about 4.4 W at 1 to 2 s. When the irradiance was 1000 W/m^2, the fluctuations were in the range of 251 to 244.7 W, with a floating range of about 6.3 W at 2 to 3 s. Figure 11(c) shows the output power simulation for the INC method control. This method improved the stability compared with the previous two tracking strategies, and although the amplitude of the oscillation was reduced, a series of oscillations were also generated when the environment changed

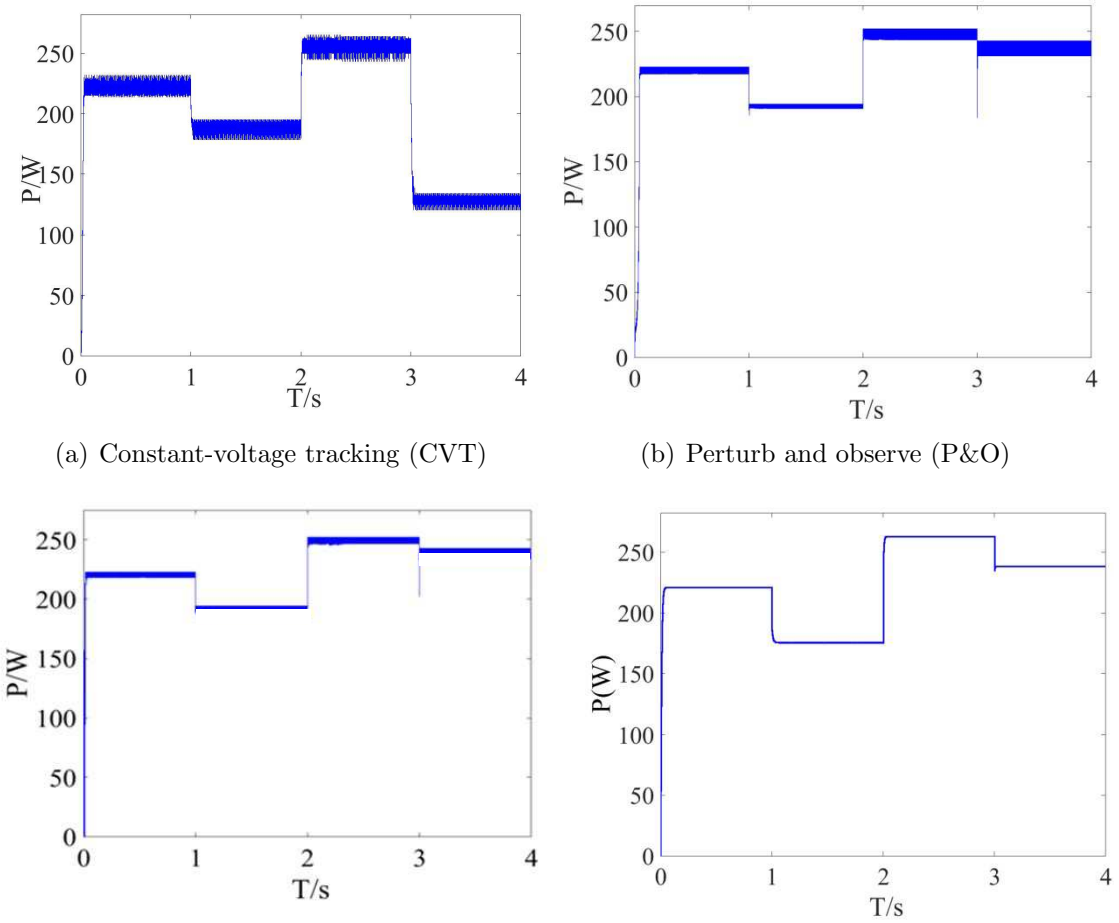

(a) Constant-voltage tracking (CVT) (b) Perturb and observe (P&O)

(c) Incremental conductance (INC) (d) Optimization algorithm

FIGURE 11. Output power curves of four algorithms

abruptly. From the overall view, the overall output power could also be more closely matched to the theoretical output maximum power case, with a floating range of about 3 to 4 W. Figure 11(d) shows the simulation diagram of the output power controlled by the improved algorithm. The improved algorithm could reduce the fluctuations of the output power caused by the environmental changes of the system. The tracking accuracy was better in the steady state, and the power output was stable at the MPP without much fluctuation. At the same time, it could track the MPP of the system more accurately and stably under situations with sudden changes of the irradiance and environment, and the fluctuation was about 0.23 W. This reduced the unnecessary power losses and thus improved the energy utilization of the PV power system.

The duty−cycle curves of the four algorithms are shown in Figure 12. The duty cycles of the conventional algorithms fluctuated to greater extents. The duty cycle of the CVT method operated in the range of 0.392 to 0.791, with a fluctuation range of about 0.325. The duty cycle of the working interval of the P&O method was between 0.623 and 0.703, and the fluctuation range was about 0.432. The duty cycle of the working interval of the INC method was between 0.683 and 0.763, and the fluctuation range was about 0.247 to 0.375. The duty cycle of the improved algorithm's working interval was between 0.723 and 0.773, and the fluctuation range was about 0.05. Therefore, the duty cycle of the improved algorithm was relatively stable. Furthermore, when the improved algorithm was in the 0 to 1 s, 1 to 2 s, and 2 to 3 s intervals, the duty cycle was around 0.75, 0.73, and

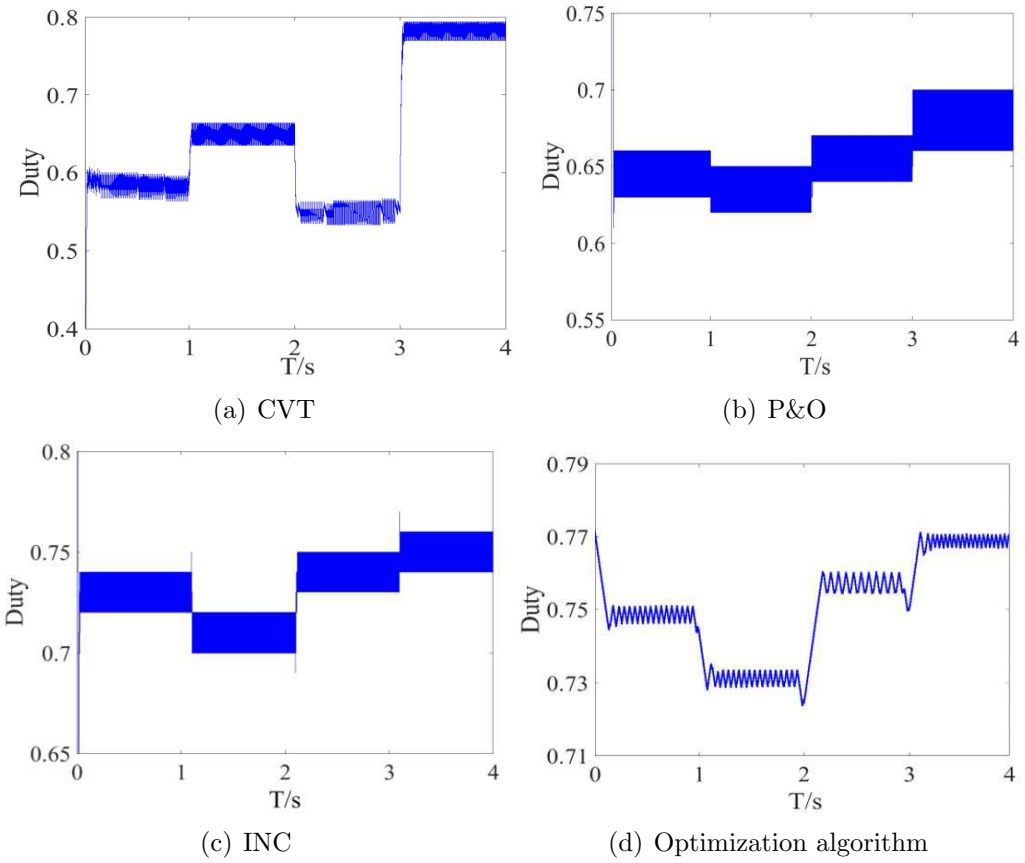

(a) CVT (b) P&O

(c) INC (d) Optimization algorithm

FIGURE 12. Duty-cycle curves of the four algorithms

0.76, respectively. When the power was at steady state, the irradiance responses were 900 W/m^2, 800 W/m^2, and 1000 W/m^2. The duty cycle results in Figure 12(d) were consistent with the maximum duty cycle of the simulated *P-D* curves under the three irradiance conditions in Figure 7(b) above.

6. **Conclusion.** 1. Based on the theoretical analysis of a PV cell, a model was built, the PV cell was simulated, and the output characteristics of the PV cell were also analyzed. The degree of influence of each factor was analyzed by varying the variables in the simulation of the PV cell output. The results showed that the power output and the maximum power output of the solar panels increased with the increase in the irradiance. Furthermore, the effect of the temperature on the efficiency of the PV generation was less than that of the irradiance. The output power and the maximum output power of the PV cell increased with the decrease in temperature.

2. To solve the problem of oscillations near the tracking speed and MPP point, a duty-cycle perturbation selection algorithm based on a hysteresis comparison was proposed. This method introduces a hysteresis comparison as the basis of the duty-cycle direction judgment. The results illustrated that the improved algorithm could better reduce the fluctuations of the system output power caused by environmental changes than the conventional algorithm. At steady state, the tracking accuracy was better and the output power was stable at the MPP without much fluctuation. In the case of sudden changes of the environment, the MPP of the system could be tracked more accurately and stably, and the fluctuation was about 0.23 W. This reduced unnecessary power losses and improved the energy efficiency of the PV power generation system.

3. The duty cycle of the conventional algorithm fluctuated widely. The duty cycle of the working interval of the CVT method ranged from 0.392 to 0.791, with a fluctuation range of about 0.325. The duty cycle of the working interval of the P&O method ranged from 0.623 to 0.703, with a fluctuation range of about 0.432. The duty cycle of the INC method ranged from 0.683 to 0.763, with a fluctuation range of about 0.247 to 0.375. The duty cycle of the improved algorithm ranged from 0.723 to 0.773, with a fluctuation range of about 0.05. The duty cycle of the improved algorithm was between 0.723 and 0.773, with a fluctuation range of about 0.05. With the optimized algorithm in the 0 to 3 s interval, the duty cycles were around 0.75, 0.73, and 0.76, respectively. It is consistent with the choice of the maximum duty cycle in Section VI, which illustrates the reasonableness of the algorithm. The duty cycle fluctuations of the proposed algorithm were less than those of all other conventional algorithms, which illustrates the feasibility of the improved algorithm with little oscillation and excellent tracking accuracy.

Acknowledgment. This entire study works were sustained by Fujian Industrial Technology Development and Application, Project No. 2021I0024.

REFERENCES

[1] I.-G. Zurbriggen, and M. Ordonez, "PV energy harvesting under extremely fast changing irradiance: State-plane direct MPPT," *IEEE Transactions on Industrial Electronics* , vol. 66, no. 3, pp. 1852-1861, 2018.

[2] V. Jately, B. Azzopardi, J. Joshi, V.-B. Venkateswaran, A. Sharma, and S. Arora, "Experimental analysis of hill-climbing MPPT algorithms under low irradiance levels," *Renewable and Sustainable Energy Reviews*, vol. 150, 111467, 2021.

[3] U. Chauhan, V. Singh, B. Kumar, and A. Rani, "An improved MVO assisted global MPPT algorithm for partially shaded PV system," *Journal of Intelligent & Fuzzy Systems*, vol. 38, no. 5, pp. 6715-6726, 2020.

[4] D. Bai, T. Zhang, and Z. Yang, "Research on improved droop control strategy of micro source inverter based on internet of things," *Security and Communication Networks*, vol. 2021, pp. 1-8, 2021.

[5] S. Li, H. Liao, H. Yuan, Q. Ai, and K. Chen, "A MPPT strategy with variable weather parameters through analyzing the effect of the DC/DC converter to the MPP of PV system," *Solar Energy*, vol. 144, pp. 175-184, 2017.

[6] L. Xu, R. Cheng, and J. Yang, "A new MPPT technique for fast and efficient tracking under fast varying solar irradiation and load resistance," *International Journal of Photo energy*, vol. 2020, pp. 1-18, 2020.

[7] R.-S. Pal, and V. Mukherjee, "Metaheuristic based comparative MPPT methods for photovoltaic technology under partial shading condition," *Energy*, vol. 212, 118592, 2020.

[8] R.-D. Silveira, G.-P. das Neves, S.-A.-O. da Silva, and B.-A. Angélico, "An enhanced MPPT algorithm based on adaptive extremum−seeking control applied to photovoltaic systems operating under partial shading," *IET Renewable Power Generation*, vol. 15, no. 9, pp. 1227-1239, 2021.

[9] A. Kihal, F. Krim, A. Laib, B. Talbi, and H. Afghoul, "An improved MPPT scheme employing adaptive integral derivative sliding mode control for photovoltaic systems under fast irradiation changes," *ISA transactions*, vol. 87, pp. 297-306, 2019.

[10] V.-R. Kota, and M.-N. Bhukya, "A novel linear tangents based P & O scheme for MPPT of a PV system," *Renewable and Sustainable Energy Reviews*, vol. 71, pp. 257-267, 2017.

[11] H.-H.-H. Mousa, A.-R. Youssef, and E.-E.-M. Mohamed, "Variable step size P&O MPPT algorithm for optimal power extraction of multi-phase PMSG based wind generation system," *International Journal of Electrical Power & Energy Systems*, vol. 108, pp. 218-231, 2019.

[12] H. Rezk, M. Aly, M. Al-Dhaifallah, and M. Shoyama, "Design and hardware implementation of new adaptive fuzzy logic-based MPPT control method for photovoltaic applications," *IEEE Access*, vol. 7, pp. 106427-106438, 2019.

[13] R.-P.-K. Naidu, and S. Meikandasivam, "Performance investigation of grid integrated photovoltaic/wind energy systems using ANFIS based hybrid MPPT controller," *Journal of Ambient Intelligence and Humanized Computing*, vol. 15, no. 5, pp. 5147-5159, 2021.

[14] J.-A. Jiang, Y.-L. Su, K.-C. Kuo, C.-H. Wang, M.-S. Liao, J.-C. Wang, and J.-C. Shieh, "On a hybrid MPPT control scheme to improve energy harvesting performance of traditional two-stage inverters used in photovoltaic systems," *Renewable and Sustainable Energy Reviews*, vol. 69, pp. 1113-1128, 2017.

[15] H.-D. Liu, C.-H. Lin, and S.-D. Lu, "A novel MPPT algorithm considering solar photovoltaic modules and load characteristics for a single stage standalone solar photovoltaic system," *IEICE Electronics Express*, vol. 17, no. 11, pp. 20200099-20200099, 2020.

[16] S. Mohanty, B. Subudhi, and P.-K. Ray, "A grey wolf-assisted perturb & observe MPPT algorithm for a PV system," *IEEE Transactions on Energy Conversion*, vol. 32, no. 1, pp. 340-347, 2016.

[17] C. González-Castaño, L.-L. Lorente-Leyva, J. Muñoz, C. Restrepo, and D.-H. Peluffo-Ordóñez, "An MPPT strategy based on a surface-based polynomial fitting for solar photovoltaic systems using real-time hardware," *Electronics*, vol. 10, no. 2, pp. 206, 2021.

[18] Y.-Q. Chen, B. Zhou, M. Zhang, and C.-M. Chen, "Using IoT technology for computer-integrated manufacturing systems in the semiconductor industry," *Applied Soft Computing*, vol. 89, pp. 1-13, 2020.

[19] Y. Peng, Q. Han, F. Su, K. He, and X. Feng, "Meteorological satellite operation prediction using a BiLSTM deep learning model," *Security and Communication Networks*, vol. 2021, no. 7, pp. 1-9, 2021.

[20] H.-D. Liu, and S.-D. Lu, "A high-performance MPPT algorithm combining advanced three-point weight comparison and temporary stopped running strategy for PV systems," *IEICE Electronics Express*, vol. 16, no. 18, pp. 1-6, 2019.

[21] X. Li, Q. Wang, H. Wen, and W. Xiao "Comprehensive studies on operational principles for maximum power point tracking in photovoltaic systems," *IEEE Access*, vol. 7, pp. 121407-121420, 2019.

[22] A.-A. El Amin, and M.-A. Al-Maghrabi, "The analysis of temperature effect for mc-Si photovoltaic cells performance," *Silicon*, vol. 10, no. 4, pp. 1551-1555, 2018.

[23] M.-C.-L Lpez-Escalante, F. Martn, and J. Ramos-Barrado, "Grouping by bulk resistivity of production-line mono-crystalline silicon wafers and its influence on the manufacturing of solar cells modules," *Solar Energy*, vol. 131, pp. 61-70, 2016.

[24] N. Gupta, N. Patel, R. Ladha, and D.-P. Saini, "A novel auto scaling variable perturbation size maximum power point tracker applied to photovoltaic (PV) system," *International Transactions on Electrical Energy Systems*, vol. 30, no. 3, pp. 1-17, 2020.

[25] T.-H. Kwan, and X. Wu, "An adaptive scale factor based MPPT algorithm for changing solar irradiation levels in outer space," *Acta Astronautica*, vol. 132, pp. 33-42, 2017.